Soil Dynamics and Earthquake Engineering 92 (2017) 239–252

Contents lists available at ScienceDirect

Soil Dynamics and Earthquake Engineering

journal homepage: www.elsevier.com/locate/soildyn

3D integrated numerical model for Fluid-Structures-Seabed Interaction (FSSI): Loosely deposited seabed foundation

Jianhong Ye[a,b,*], D.-S. Jeng[c], A.H.C. Chan[d], R. Wang[a], Q.C. Zhu[a]

[a] State Key Laboratory of Geomechanics and Geotechnical Engineering, Institute of Rock and Soil Mechanics, Chinese Academy of Sciences, Wuhan 430071, China
[b] Division of Civil Engineering, University of Dundee, Dundee DD1 4HN, UK
[c] Griffith School of Engineering, Griffith University, Gold Coast, Queensland 4222, Australia
[d] School of Information and Communication Technology, University of Tasmania, Hobart, Australia

ARTICLE INFO

Keywords:
Fluid-Structures-Seabed Interaction (FSSI)
Loosely deposited seabed foundation
3D residual liquefaction
Caisson breakwater
PZIII
FSSI-CAS 3D

ABSTRACT

In the past several decades, a great number of offshore structures have been constructed on loosely deposited seabed foundation because sometimes there would be no a dense seabed floor could be chosen in planned sites, for example, the breakwaters and oil platforms in the Yellow River estunary area, China. Wave-induced residual liquefaction is easy to occur in loosely deposited seabed, which brings great risk to the stability of offshore structures. In this study, we focus our attention on the 3D interaction mechanism between ocean wave, a caisson breakwater and its loosely deposited seabed foundation. A three-dimensional integrated numerical model FSSI-CAS 3D is taken as the computational tool; and the soil constitutive model: Pastor-Zienkiewicz Mark III (PZIII) proposed by Pastor et al. [16] is adopted to describe the wave-induced dynamic behavior of loose seabed soil. The numerical results indicate that the developed integrated numerical model FSSI-CAS 3D is capable of capturing a series of nonlinear phenomena, such as tilting, subsiding of breakwater, as well as residual liquefaction in loose seabed foundation etc., in the interaction process between ocean wave, a caisson breakwater and its loose seabed foundation. The purpose of this study is to provide coastal engineers with comprehensive understanding of FSSI problme involving loosely deposited seabed soil; and propose a reliable computational method to engineers involved in the design of offshore structures on loose seabed foundation.

1. Introduction

There are a great deal of newly deposited Quaternary loose sediment in offshore area in the world, for example, the Yellow River estunary area in China. An important characteristics of these offshore Quaternary sediment is that soil particles are relatively loose; and their relative density D_r is small. As a result, these Quaternary offshore soils has low P wave speed, and low SPT (Standard Penetration Test) value; and their bearing capacity is also weak. From the perspective of engineering practice, offshore Quaternary sediment is not an ideal choice as the foundation of offshore structures. The main reason can be attributed to the fact that Quaternary loose sediments are easy to liquefy under ocean wave or seismic wave loading. It is well known that a liquefied seabed soil behaves like a kind of heavy fluid; it can not support any overlying structure. As a result, offshore structures built on Quaternary loose sediment are more suspectable to lost stability during their usage lifetime under ocean/seismic wave loading. Sometimes, coastal engineers have to face the situation that there is no other choice in a planned site. Under the situation that a Quaternary sediment seabed has to be chosen as the foundation of designed offshore structures, evaluation of the stability of designed offshore structures under ocean/seismic wave is apparently necessary. This stability evaluation for offshore structures must be based on comprehensive investigation of the complicated interaction between ocean wave, offshore structures and their loose seabed foundation. In the engineering of practice, it is desirable that if there is a reliable numerical model available for this purpose.

Currently, there are some investigations on the topic of wave-induced dynamics of elasto-plastic sand soil, and related marine structures available. The investigation methods include decoupled analytical solution [17,2,21], decoupled numerical modelling [12,3,19,20], as well as laboratory test [18,10,35,5,11]. In these analytical solutions, a source term function was added to pore pressure dissipation equation to approximately describe the mechanism of pore

* Corresponding author at: State Key Laboratory of Geomechanics and Geotechnical Engineering, Institute of Rock and Soil Mechanics, Chinese Academy of Sciences, Wuhan 430071, China.
E-mail address: yejianhongcas@gmail.com (J. Ye).

http://dx.doi.org/10.1016/j.soildyn.2016.10.026
Received 7 October 2015; Received in revised form 18 August 2016; Accepted 17 October 2016
Available online 18 November 2016
0267-7261/

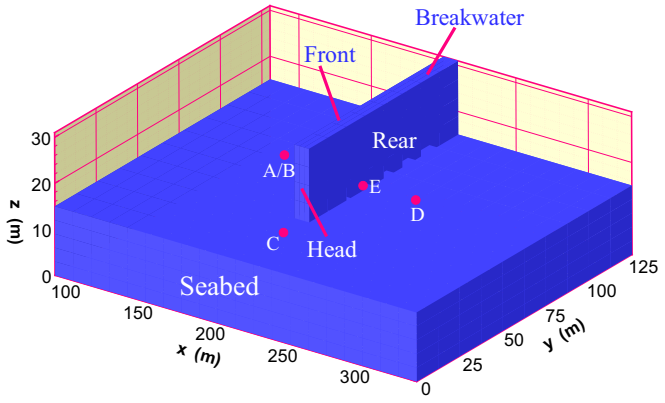

Fig. 1. Configuration of chosen computational domain. A caisson breakwater (Length×Width×Height=90 m×10 m×16 m) is constructed on a loose seabed foundation. The dimension of seabed is Length×Width×Height=250 m (x=80–330 m)×130 m×15 m. The position of the caisson breakwater is x=200–210 m, y=40–130 m, z=15–31 m. Five typical positions labelled as A–E around the breakwater head are chosen in results analysis. Their projection on plane z=15 m are shown.

pressure build-up. Actually, the simplified source term function based on constant magnitude of wave-induced shear stress is unlikely to describe the mechanism accurately, for example, it generally assumes that the magnitude of wave-induced shear stress in loose seabed soil was constant. This assumption is obviously unreasonable because the shear stress will gradually reduce to zero in the liquefaction process [29,34]. As a result, the predicted pore pressure is not reliable. They can not agree with experimental data in most cases. Additionally, analytical solutions can not handle complex boundary conditions and soil constitutive models; and the variation of effective stress also can not be determined in computation. Numerical models have the natural advantages to handle complex boundary conditions and soil constitutive models. However, linear or nonlinear Stokes wave was utilized to apply wave loading on seabed floor in previous literature. The fluid-structures interaction, and the fluid exchange between sea water and pore water in loose seabed also were not taken into consideration. As an integrated system between ocean wave, offshore structures and their loose seabed foundation, a coupled numerical model should be used to investigate their interaction. Ye et al. [33] developed a semi-coupled numerical model FSSI-CAS 2D for this purpose; and this model has been validated by a wave flume test [22] and a centrifuge test [18]. Based on the fact that most previous numerical models for FSSI problem are limited to 2D, Ye et al. [32] further extended 2D package to form FSSI-CAS 3D. At present, FSSI-CAS 3D is capable of investigating the complicated interaction between ocean wave, offshore structures and their loose seabed foundation.

Table 1
Properties and parameters used for seabed foundation, composite breakwater and wave in analysis and parametric study.

Parameters for PZ3 model (from Nevada sand)		
Item	Value	Unit
K_{evo}	2,000	[kPa]
G_{eso}	2,600	[kPa]
p_0	4	[kPa]
M_g	1.32	–
M_f	1.3	–
α_f	0.45	–
α_g	0.45	–
β_0	4.2	–
β_1	0.2	–
H_0	750	–
H_{UO}	40,000	[kPa]
γ_u	2.0	–
γ_{DM}	4.0	–
Soil characteristics		
Soil permeability (k)	1.0×10^{-5}	[m/s]
Poisson's ratio (ν)	0.3333	
Saturation (S_r)	95, 98 or 100	%
Porosity (n)	0.25	
Relative density (D_r)	60%	
Breakwater		
Permeability (k)	1.0×10^{-10}	[m/s]
Poisson's ratio (ν)	0.25	
Saturation (S_r)	0	%
Young's modulus (E)	1.0×10^4	[MPa]
Porosity (n)	0.1	
Wave characteristics		
Wave height	1.5	[m]
Wave period	8.0	[s]
Water depth	10	[m]

In this study, the configuration of breakwater and its seabed foundation is shown in Fig. 1. As shown in Fig. 1, a caisson breakwater is constructed on a loosely deposited seabed foundation. The wave-induced dynamics of the loose seabed foundation around the caisson breakwater is investigated in an integrated way, by adopting FSSI-CAS 3D. The wave-induced pore pressure build up, variation of effective stresses, and residual liquefaction potential in loose seabed foundation are the focus of this study. The purpose is to provide engineers with comprehensive understanding of FSSI problem involving loosely deposited seabed foundation; and propose a reliable computational method to coastal engineers involved in the design of offshore structures on loose seabed.

2. Integrated numerical model and constitutive model

The integrated numerical model FSSI-CAS 3D for fluid-seabed-structures interaction contains two modules: wave model and soil model. The wave model is responsible for the generation, propagation of wave, and determines the pressure acting on seabed and marine structures in computation. The modified Navier-Stokes equations are the governing equation for wave motion on seabed, and its interaction with marine structures, as well as porous flow in loose seabed. They are solved by using a FVM-based N-S solver provided by the open source code TRUCHAS (2009) developed by US Los Alamos National Laboratory (LANL). In TRUCHAS, VOF method is adopted to trace the free surface of wave motion. The drag force between pore fluid and solid matrix is formulated as $F_{di} = C_d \frac{\nu}{d_{50}^2} \frac{(1-n)^2}{n^2} u_{fi}$ [7]. In this wave model, the internal wave maker proposed by Lin and Liu [13] is applied to generate the target wave train, in which a mass function is added to the continuity equation at the position where the wave maker is located. The soil model determines the dynamic response of seabed and marine structures taking the wave-induced pressure/force on seabed and marine structures determined by wave model as the boundary value. The dynamic Biot's equation known as 'u-p' approximation is the governing equation for dynamics of soil and structures. It is solved adopting a FEM-based solver, in which Generalized Newmark-β method is used for time integration, and Newton-Raphson method is used for global iteration.

In this integrated numerical model, the non-match mesh scheme and non-match time step are used in coupling computation. A data exchange port is developed adopting 3D Shepard interpolation method to transmit data at the interface between fluid domain and solid domain. In the integrated model, pressure and flux continuity on interfaces between fluid domain and solid domain is applied all the time in computation. More information about the integrated model FSSI-CAS 3D can be found in Ye et al. [33].

It seems to be that a monolithical scheme [1] is used in computation. There is no feedback from solid domain to fluid domain. Actually, the coupling between the wave model and soil model can be referred to as a semi-coupling process [33], because the seabed foundation is considered as porous medium in wave model when determining wave

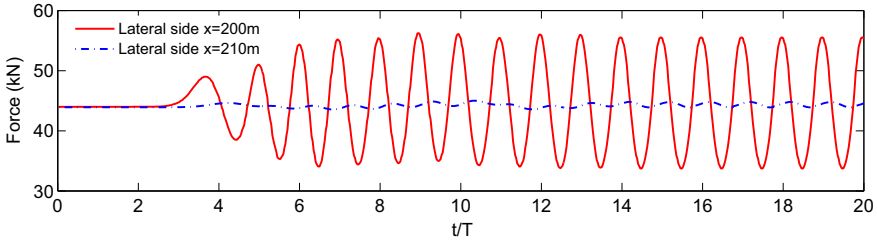

Fig. 2. Wave-induced force on the front and rear lateral sides of the caisson breakwater.

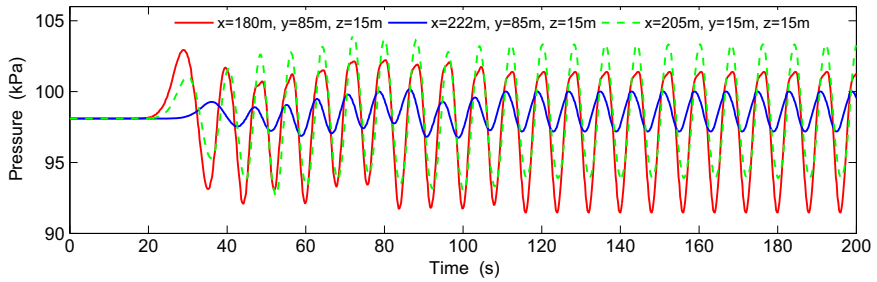

Fig. 3. Wave-induced dynamic pressure acting on the seabed foundation around the head of caisson breakwater.

field; the effect of porosity of seabed foundation on wave field has been taken into consideration. Therefore, the flow field in fluid domain and solid domain is continuous at their interfaces. However, the displacement at interfaces is not continuous. From the point view of physics, the wave-induced vibration of marine structures and seabed foundation generally is apparently minor comparing with the wave length. The discontinuity of displacement between fluid domain and solid domain is acceptable if there is no large deformation involved. If displacement continuity on interfaces must be implemented through iterative process (also referred as to staggered scheme [4]), the computation will be very expensive. Additionally, as far as we know, there is no a code so far can implement the fully coupled computation for fluid-seabed-structures interaction problem.

The developed 3D integrated numerical model FSSI-CAS 3D has been validated by an analytical solution [6] and a laboratory wave flume tests [14] for the problem of ocean wave-marine structure-dense seabed foundation interaction [32]. The verification of FSSI-CAS 2D for the problem of ocean wave-loose seabed interaction also has been conducted in Ye et al. [33]. Due to the fact that FSSI-CAS 3D is developed under the same frame of FSSI-CAS 2D, it is certainly sure that FSSI-CAS 3D is applicable for the problem of wave-loose seabed-marine structures interaction.

Quaternary newly deposited loose sediments widely exist in offshore area. Under cyclic loading, soil compaction due to uncoverable plastic volumetric deformation would occur in loose sediments. In this study, an advanced elasto-plastic constitutive model: Pastor-Zienkiewicz Mark III (PZIII) proposed by Pastor et al. [16] is adopted to describe the wave-induced dynamic behavior of loose seabed soil. PZIII is an excellent constitutive model to describe the behaviors of clay and sandy soil. Its reliability has been validated by a series of laboratory tests involving monotonic and cyclic loading [36], especially in the project VELACS. This model is one of the heritage of Olek Zienkiewicz [15]. More information about PZIII model can be found in Pastor et al. [16, 36]. Previous investigation conducted by Ye et al. [27] has evidently proved that PZIII model is capable of modelling the wave-induced dynamics of loose seabed foundation. A series of physical mechanism of loose soil to cyclic loading revealed by experimental tests can be effectively captured by PZIII model.

3. Boundary condition applied

In computation, the bottom of loose seabed foundation is fixed; and the lateral sides are only fixed in horizontal direction. On the surface of seabed, the wave-induced pressure and hydrostatic pressure are applied instantaneously. At the meantime, the pore pressure in seabed foundation and the water pressure in seawater are continuous on the surface of seabed, guaranteeing the effective stresses on seabed surface is zero all the time. The caisson breakwater is applied by the wave-induced pressure and hydrostatic pressure on its lateral sides; and its bottom is applied by upward buoyant. The caisson breakwater is

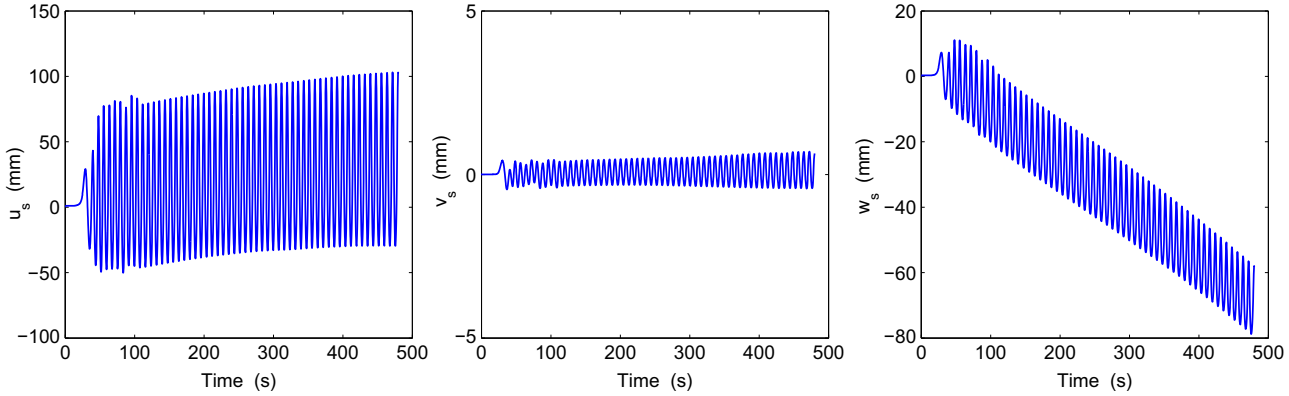

Fig. 4. Displacement of caisson breakwater on loosely deposited seabed foundation under wave loading.

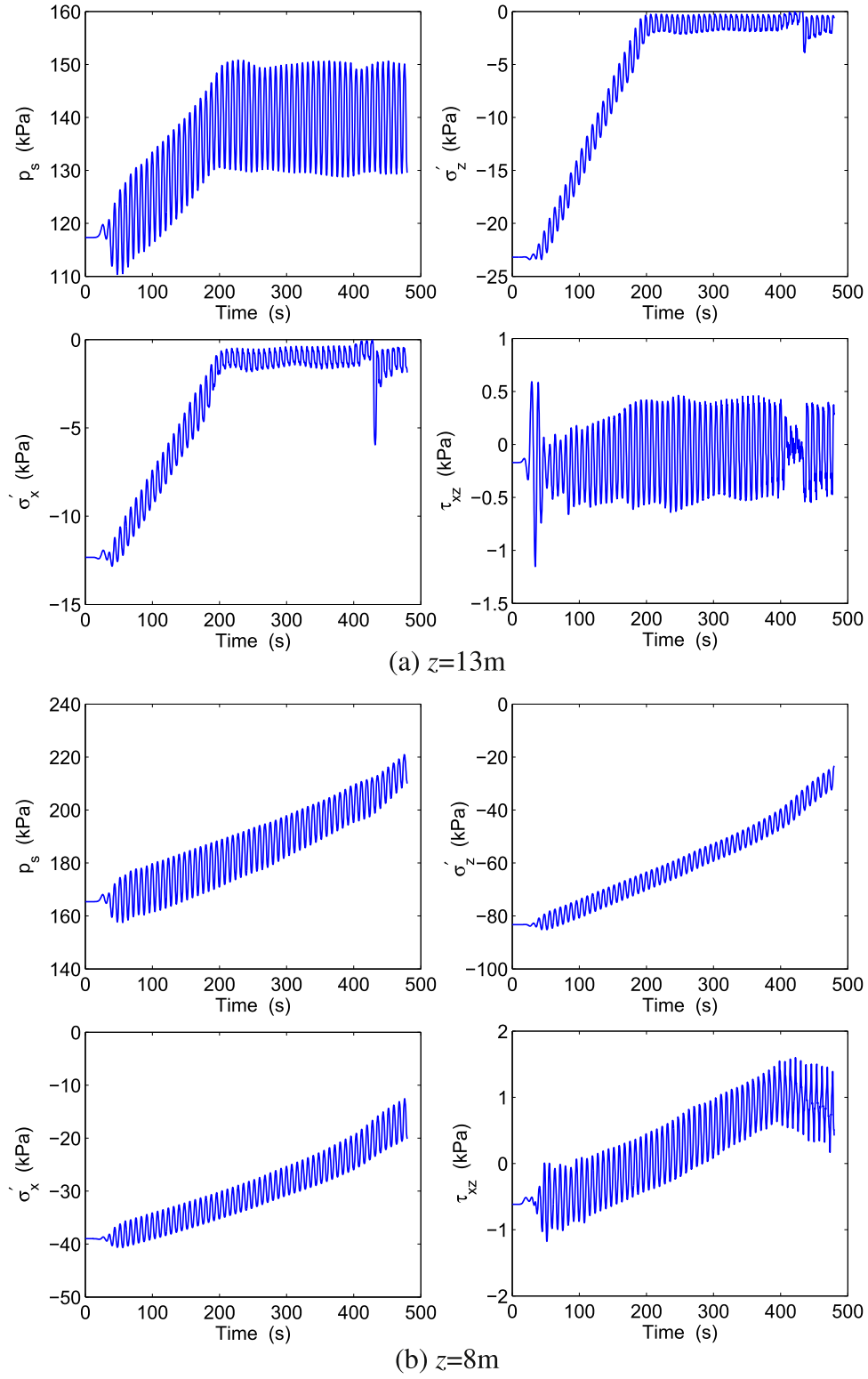

Fig. 5. Pore pressure build up, and effective stresses reduction at typical positions in front of the breakwater due to the standing wave loading. (a): A (x=164 m, y=85 m, z=13 m); (b): B (x=164 m, y=85 m, z=8 m), (a) z=13 m (b) z=8 m.

treated as a rigid body with apparent small permeability.

4. Dynamic response of caisson breakwater

The parameters of wave characteristics for wave maker here are: H=1.5 m, d=10.0 m, and T=8.0 s. In CFD computation, a series of absorption zones are set to absorb the wave energy on boundaries, avoiding the unexpected wave reflection. The property parameters of seabed soil for PZIII model in computation are listed in Table 1. They were determined by Zienkiewicz et al. [36] from the laboratory tests of Nevada sand in the VELACS project funded by American National Science Foundation (NSF). Here, the parameters from Nevada sand just is an example in this numerical simulation. For a real seabed soil, engineers must conduct laboratory tests on soils sampled from seabed

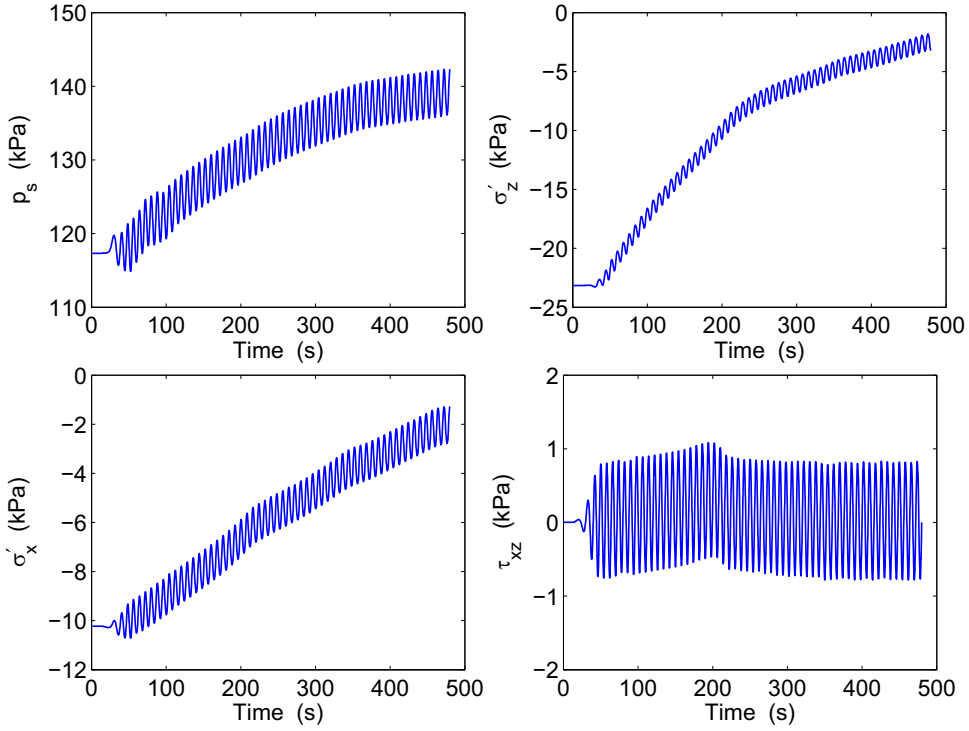

Fig. 6. Pore pressure build up, and effective stresses reduction at typical position C (x=205 m, y=15 m, z=13 m) near to the breakwater head due to the progressive wave loading.

foundation, to determine the mechanical parameters for PZIII model or other constitutive models.

Taking the consolidation state of the seabed foundation under the caisson breakwater and hydrostatic pressure determined as that in Ye et al. [31], as the initial condition, wave-induced dynamics of the caisson breakwater, and its loosely deposited seabed foundation is investigated in the followings. In this study, it is stipulated that compression is taken as negative value; and displacement is taken as positive value if it is in $+x$, $+y$, $+z$ direction.

There are three kinds of wave field around the caisson breakwater: standing wave in front of the caisson breakwater, diffracted wave behind the caisson breakwater, and progressive wave near to the breakwater head. Wave impact on the caisson breakwater applied by designed wave is an important factor need to be considered in design of marine structure. Fig. 2 demonstrates the ocean wave-induced force on the front and rear lateral sides of the caisson breakwater. It is clearly

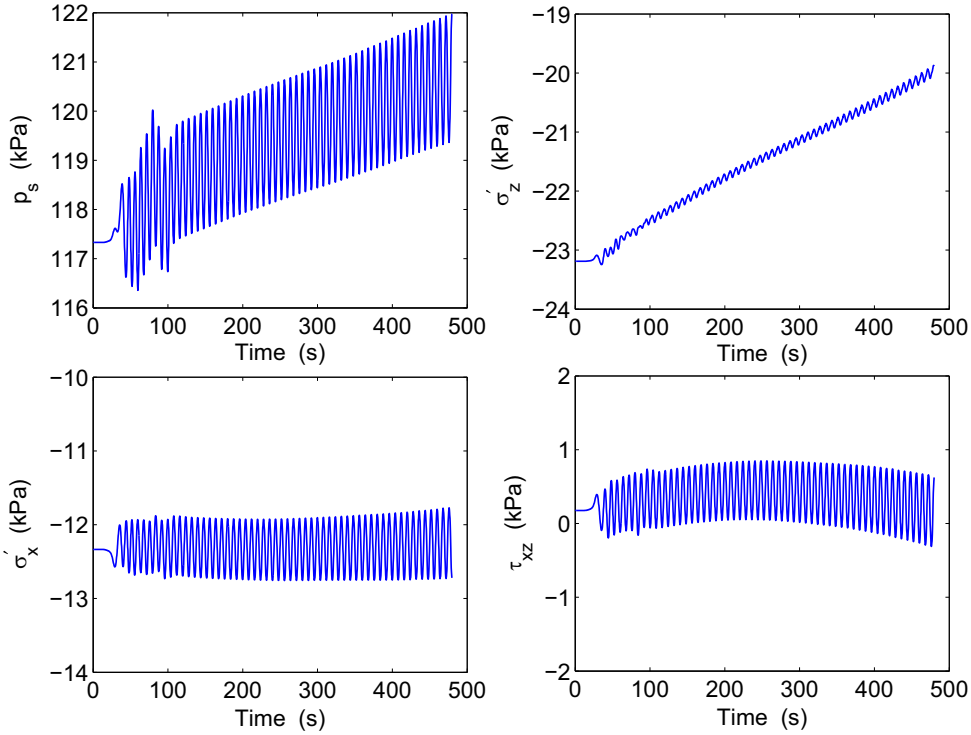

Fig. 7. Pore pressure build up, and effective stresses reduction at typical position D (x=246 m, y=85 m, z=13 m) behind the breakwater due to the diffracted wave loading.

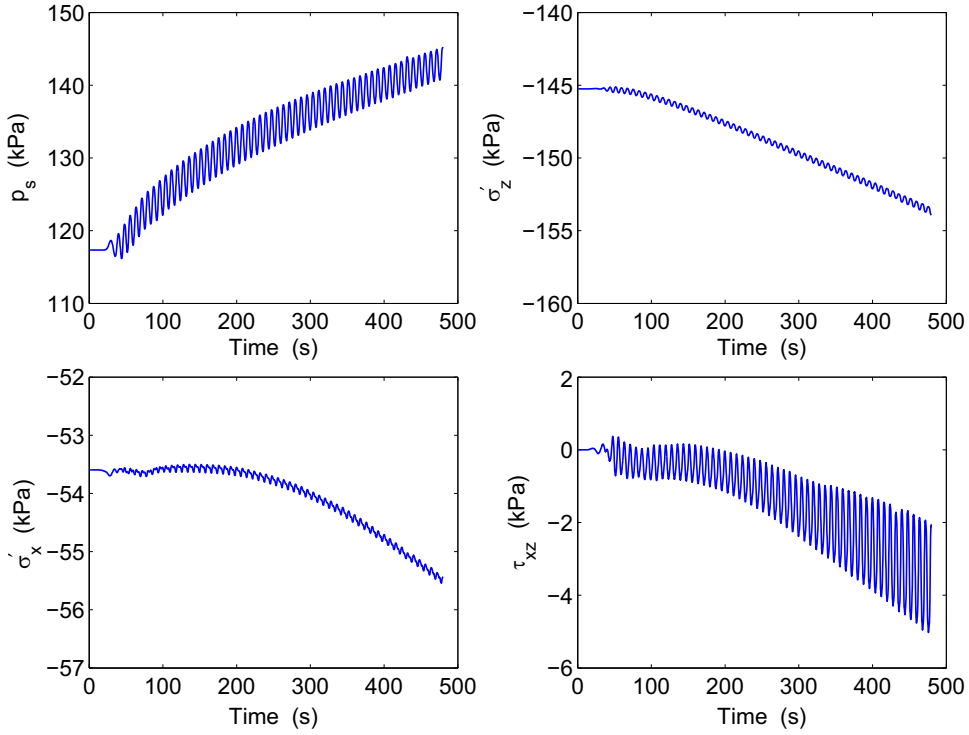

Fig. 8. Pore pressure build up, and effective stresses reduction at typical position E (x=205 m, y=85 m, z=13 m) under the breakwater.

seen that the wave-induced force acting on the front lateral side of the caisson breakwater is much greater than that on its rear lateral side. Fig. 3 shows the wave-induced dynamic pressure acting on the seabed foundation around the head of caisson breakwater. It is clearly observed that wave-induced dynamic pressure acting on the seabed in front of the breakwater, and near to breakwater head is also much higher than that behind the breakwater. It is indicated that the standing wave in front of the caisson breakwater, and the progressive wave near the breakwater head play a dominant role for the dynamics of the caisson breakwater and its seabed foundation.

Fig. 4 illustrates the wave-induced displacements of the caisson breakwater constructed on the loosely deposited seabed foundation. It can be found that the caisson breakwater mainly vibrates to $+x$ and $-x$ direction periodically. The vibration amplitude is about 70 mm. It is indicated that wave-induced dynamic response of breakwater on a loose seabed foundation is much stronger than that on a dense seabed foundation. Additionally, the caisson breakwater has a permanent horizontal displacement toward to $-x$ direction (reach up to 50 mm). This is significantly different with that if the caisson breakwater is built on a dense seabed foundation [28], in which there is no residual displacement. Another phenomenon observed in Fig. 4 is that the caisson breakwater gradually subsides, which is attributed to soil compaction resulted from the rearrangement of soil particles under cyclic loading. This is a unfavorable factor for the stability of breakwater built on loose seabed foundation. In general, the construction of a marine structure on loosely deposited seabed is much more dangerous than that on dense seabed.

5. Dynamic response of seabed foundation

It has been widely recognized that pore pressure could builds up, and effective stresses reduces in a poro loose seabed foundation resulted from cyclic wave loading. However, how the caisson breakwater affects pore pressure build up, and effective stresses reduction in the region around a breakwater head is not fully understood so far. In this section, the effect of the caisson breakwater on pore pressure and effective stresses in loose seabed foundation is investigated. Five typical positions are chosen as the representatives for the analysis: A (x=164 m, y=85 m, z=13 m) in front of the breakwater, B (x=164 m, y=85 m, z=8 m) in front of the breakwater, C (x=205 m, y=15 m, z=13 m) near to the breakwater head, D (x=246 m, y=85 m, z=13 m) behind the breakwater, and E (x=205 m, y=85 m, z=13 m) under the breakwater.

Figs. 5–8 illustrate the time history of pore pressure build up, and effective stresses reduction at the five chosen positions around the caisson breakwater. In Fig. 5(a), it can be seen that the pore pressure at A does not continuously build up after t=200 s. The residual pore pressure basically keep 23 kPa; and the magnitude of oscillatory pore pressure is about 10 kPa after t=200 s. Meanwhile, effective stress σ_x and σ_z nearly approaches zero from their initial compressive state. Under such situation, it is indicated that the seabed soil at position A in front of the breakwater becomes liquefied after t=200 s. In Fig. 5(b), it is found that although the wave-induced residual pore pressure at B reaches up to about 47 kPa, much greater than that at A, the effective stresses σ_x and σ_z are still far away from the zero stress state (complete liquefaction state). This is attributed to the fact that buried depth of position B is much deeper than that of position A. The initial self-gravity induced effective stresses at position B is much greater than that at position A. It makes the soil at B is much more difficult to liquefy.

In Figs. 6 and 7, it is found that pore pressure in the seabed near at position C to the breakwater head, and at position D behind the breakwater continuously builds up in the whole process of wave loading. Correspondingly, effective stresses between soil particles at the two positions continuously reduce. This phenomenon is significantly different with that in front of the caisson breakwater. There is a gap to the zero stress (full liquefaction state) at position C and D. The difference to zero vertical effective stress is about 2.5 kPa and 20 kPa, respectively at the two typical position C and D. It is indicated that the seabed soil near to the breakwater head is much easier to liquefy than the soil behind the breakwater. At the end of computation, the wave-induced residual pore pressure is about 23 kPa at position C, which is the same with that at position A shown in Fig. 5. However, the time to reach this magnitude of residual pore pressure at position C lags about

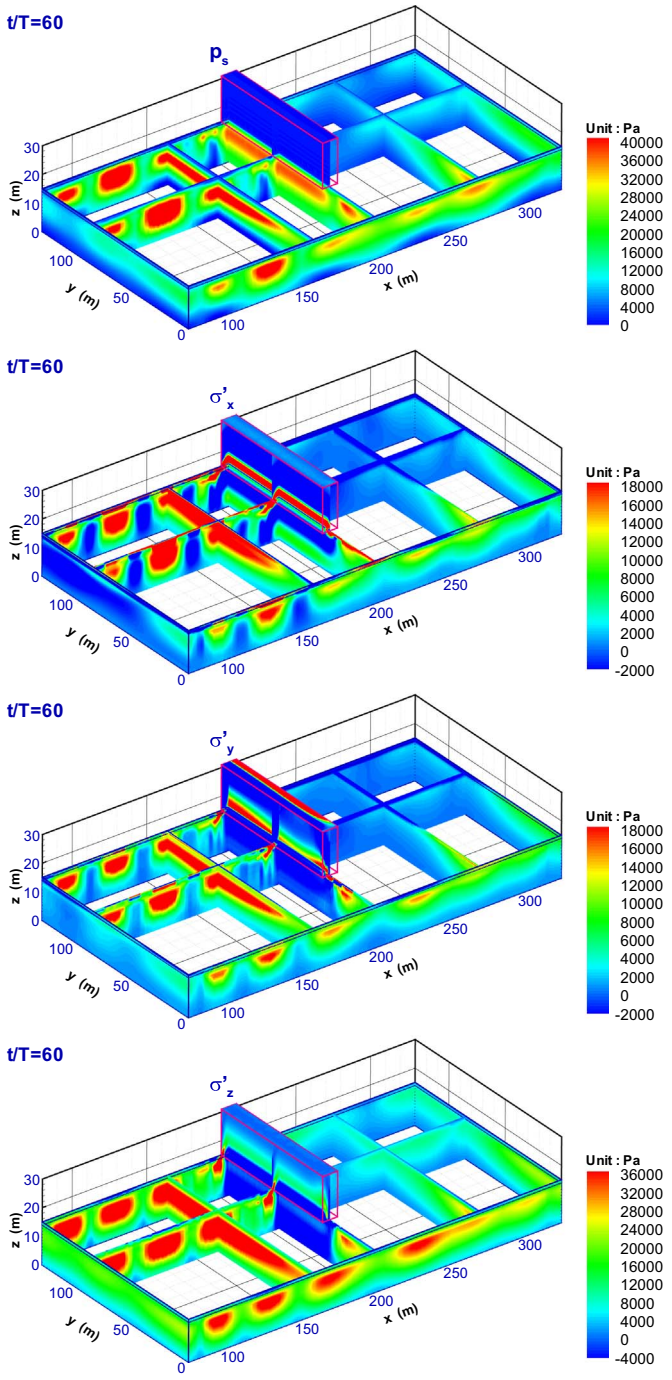

Fig. 9. Distribution of the 3D wave-induced excess pore pressure and the corresponding dynamic effective stresses in the seabed foundation at time t/T=60.

35 wave periods. It is indicated that the seabed response in front of the breakwater is much stronger than that near to the breakwater. At position D, the wave-induced residual pore pressure is only 3 kPa, which is much smaller than that at A and C. It is shown that the wave-induced seabed response is weakest behind the caisson breakwater. Comparing with the characteristics of wave field around the caisson breakwater, it is found that the dynamic response of seabed foundation is directly related to the wave field distribution.

It is interesting to reveal the dynamic response of seabed foundation under the caisson breakwater. Obviously, there is no direct wave loading on the seabed surface under the caisson breakwater (contact with the bottom of breakwater). However, the vibration of pore pressure at the interface between the seabed foundation and the caisson breakwater, as well as the wave-induced swaying of the caisson breakwater have significant effect on the seabed dynamics under the caisson breakwater. Fig. 8 illustrates the time history of wave-induced pore pressure, effective stress σ_x, σ_z, and shear stress τ_{xz} at the representative position E beneath the caisson breakwater. It can be seen that the pore pressure also builds up. The wave-induced residual pressure reaches up to 26 kPa, which is actually greater than that at position A and C even they have the same buried depth. However, the effective stresses and shear stress in seabed foundation under the caisson breakwater increase in the process of wave loading at the meantime. This phenomenon is completely different with that in other zones around the caisson breakwater. The reason for this phenomenon is attributed to the effect of swaying and tilting of breakwater. As mentioned in above section, wave impact acting on the lateral sides of the caisson breakwater makes the breakwater built on loose seabed foundation sway. The swaying of breakwater makes the soil particles beneath it rearranges more easily accompanying the pore water drainage, and makes the soil particles contact with each other more densely. Soil compaction due to the rearrangement of soil particles makes the pore pressure under the breakwater builds up. At the meantime, the offset to $-x$ direction of gravity center, as well as gravity compression of breakwater makes the contact effective stresses, and shear stresses between soil particles at position E become greater and greater. This highly nonlinear phenomenon also has been observed more clearly in Ye and Wang [34] and Ye et al. [26].

Fig. 9 demonstrates the distribution of wave-induced excess pore pressure and corresponding dynamic effective stresses in the loose seabed foundation at time $t/T = 60$. In Fig. 9, it is found that wave-induced pore pressure in the zones under the nodes of standing wave is much higher than that in the zones under the anti-nodes of standing wave in front of the caisson breakwater; the influence depth of the standing wave is much deeper than that of the progressive wave near to the breakwater head. It is also can be seen that diffracted wave-induced pore pressure is smallest behind the caisson breakwater. It is indicated that protection of the caisson breakwater for the seabed behind it is effective. In the regions where pore pressure significantly building up, the wave-induced dynamic effective stress σ_x, σ_y and σ_z are tensile (positive value). It means that the effective stresses reduce significantly, and potentially reach or approach liquefaction state. Attention is paid to the zone under the caisson breakwater. It is clearly observed that there is a high residual pore pressure zone beneath the breakwater; however, the dynamic effective stresses in this zone is not tensile, but compressive (negative value). It is again indicated that soil particles

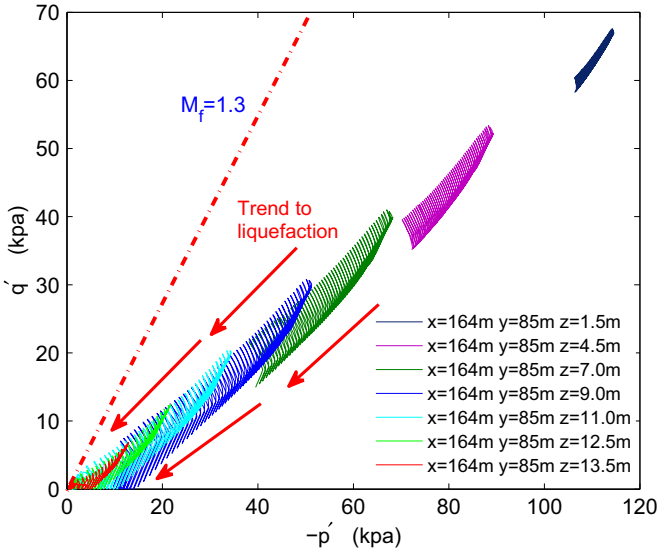

Fig. 10. Stress path along the depth of seabed foundation on line x=164 m, y=85 m (in front of the caisson breakwater). M_f is the slope of the yield surface on $p' - q'$ plane.

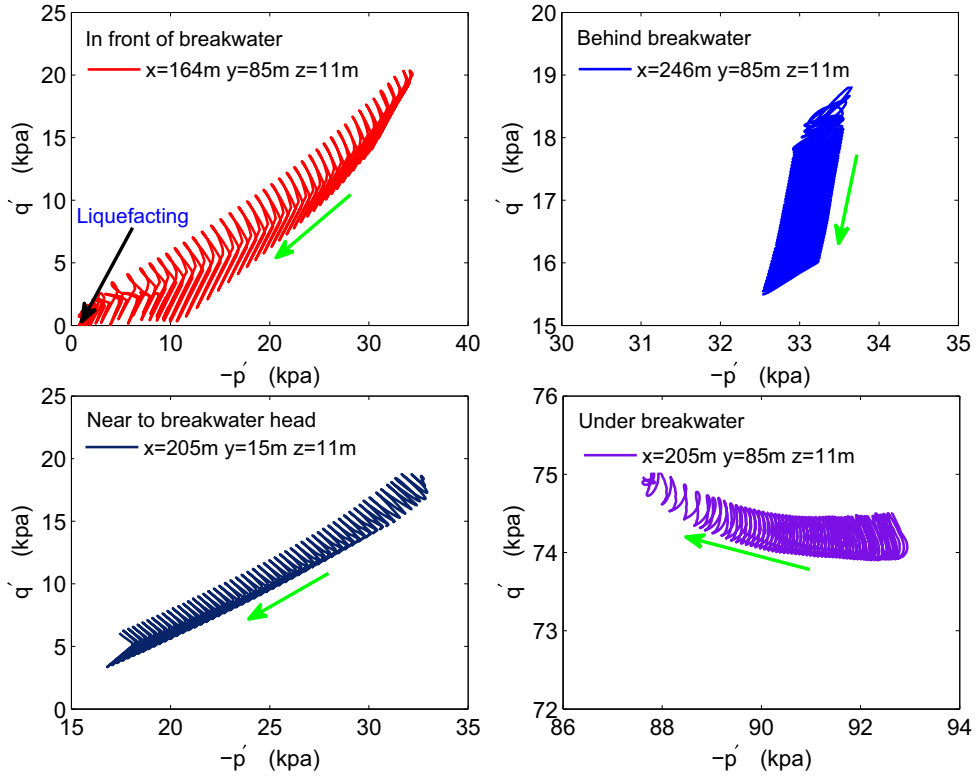

Fig. 11. Stress path on four typical points in the seabed foundation around the caisson breakwater on the horizontal plane z=11 m.

under the caisson breakwater contact more densely relative to its initial consolidation state.

6. Progressive liquefaction in seabed foundation

6.1. Definition of progressive liquefaction and criterion

It is well known that there are two kinds of mechanism for sand liquefaction corresponding to dense seabed (poro-elastic) and loose seabed (poro-elastoplastic): momentary liquefaction and residual liquefaction. The momentary liquefaction only can occur in very dense seabed. In this section, wave-induced residual liquefaction in loose seabed foundation around the caisson breakwater is investigated. The essence of residual liquefaction of sand bed is that soil particles are loosely deposited in offshore area. Under cyclic loading, such as ocean wave or seismic wave, soil particles trend to rearrange their relative positions, resulting in pore pressure build up, and effective stress reduction in soil if the drainage of pore water is poor. When wave-induced residual pore pressure is sufficient to make the contact effective stresses between soil particles become zero, seabed soil becomes liquefied. The wave-induced residual liquefaction in sand bed does not appear and disappear periodically like the momentary liquefaction, but is a progressive process. This progressive liquefaction process has been observed in a centrifuge test by Sassa and Sekiguchi [18]. The liquefaction in loose seabed first occurs at the surface of seabed; then, the frontier of liquefaction zone advances downward gradually under wave loading.

Soil liquefaction is actually a process for effective stresses to reduce and approach zero stress state. Generally, liquefaction process can be reflected by stress path plotting. Fig. 10 shows the stress paths along the depth of the loose seabed foundation on line x=164 m, y=85 m (in front of the caisson breakwater). It is observed that the magnitude of initial stress has positive relation with buried depth; and the mean effective stress p' and deviatoric stress q' both reduce in the process of wave loading. At the end of computation, only the soil in the upper seabed can reach the zero stress state. The soil in the lower seabed is far away from liquefaction state.

Fig. 11 illustrates the stress paths on four typical points around the caisson breakwater on the plane z=11 m. It is clearly observed that the mean effective stress p' and deviatoric stress q' at the point in front of the breakwater gradually reduce, and finally reach liquefaction state under standing wave loading. p' and q' at the points near to the breakwater head, and behind the breakwater also reduce; however, they are finally still far away from the zero stress state. It is interesting to point out that p' is reduced; while q' is increased at the position under the breakwater. The reduction of p' is due to the pore pressure build up, as illustrated in Fig. 8; the increasing of q' is due to the swaying and tilting of the breakwater. The seabed soil at position E contributes more and more bearing capacity to support its overlying breakwater. It is indicated that the soil under the caisson breakwater is unlikely to liquefy due to the compression of the breakwater.

$$\sigma_z + 2(c - \sigma_x \tan\phi)u(-\sigma_x) + 2(c - \sigma_y \tan\phi)u(-\sigma_y) \geq 0 \tag{1}$$

in which $u(x)$ is the unit step function

$$u(x) = \begin{cases} 1 & x > 0 \\ 0 & x \leq 0 \end{cases} \tag{2}$$

where c and ϕ is the cohesion and internal friction of soil. σ_x, σ_y and σ_z are the current effective stress (compression is negative). For sandy soil, its cohesion c normally is 0. Ye [30] claims that the 3D liquefaction criterion proposed by Tsai [23] is a special form of the above proposed liquefaction criterion when c=0 and ϕ=26.6°. However, the above liquefaction criteria considering friction between soil particles is only established for momentary liquefaction. For residual liquefaction, friction between soil particles actually has no contribution to liquefaction resistance in loose seabed soil; while cohesion has significant contribution to residual liquefaction resistance, for example, clay soil generally is difficult to be liquefied even residual pore pressure has exceeded initial vertical effective stress σ_{z0}. Based on this mechanism, and considering $\sigma_z = \sigma_{z0} + \sigma_{zd}$, where σ_{z0} is the initial vertical effective

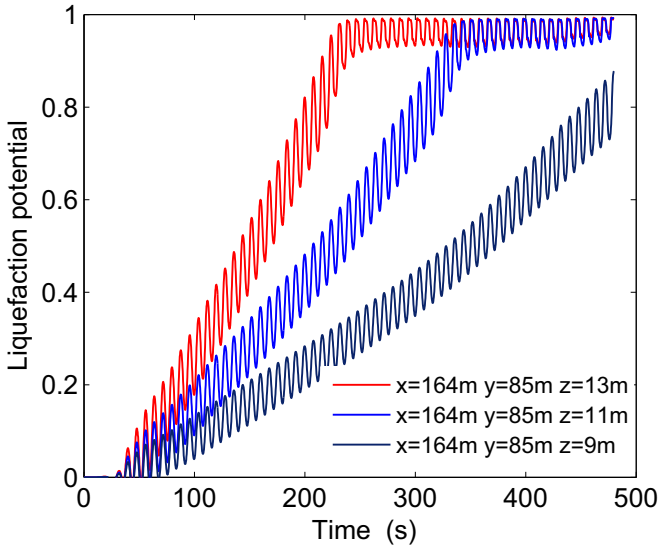

Fig. 12. Liquefaction potential at typical position on line (x=164 m, y=85 m) in front of the breakwater (noted: passing through position A and B).

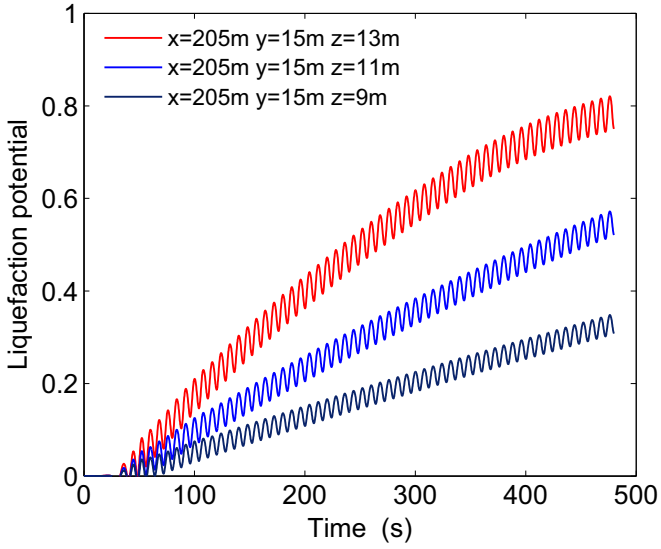

Fig. 13. Liquefaction potential at typical positions on line (x=205 m, y=15 m) near to the head of the breakwater (noted: passing through position C).

stress, and σ_{zd} is the wave-induced dynamic vertical effective stress, the residual liquefaction potential is defined as

$$L_{potential} = \frac{\sigma_{zd}}{-\sigma_{z0} + \alpha c} \tag{3}$$

where α is a material coefficient. Due to the fact that macroscopic cohesion c of seabed soil is not absolutely equivalent to the microscopic liquefaction resistance of soil particles, a material coefficient must be added to cohesion c of soil in Eq. (3). Currently, investigation on the effect of cohesion of soil on its liquefaction resistance is limited. As a result, the value of material coefficient α is not sure. This will be a interesting topic in the future.

In theory, when $L_{potential}$ is greater than or equal to 1.0 at a position, the soil is liquefied at this position. Obviously, liquefaction potential of soil would be overestimated if the cohesion of soil are not taken into consideration in analysis. But actually, $L_{potential}$ will never exceed 1.0 either in numerical computation or in laboratory tests [8,24]. The reason is that sand soil is non-cohesive granular material. It can not bear any tensile stress. Therefore, a sandy soil can not reach the complete liquefied state in numerical computation. Namely, the ratio

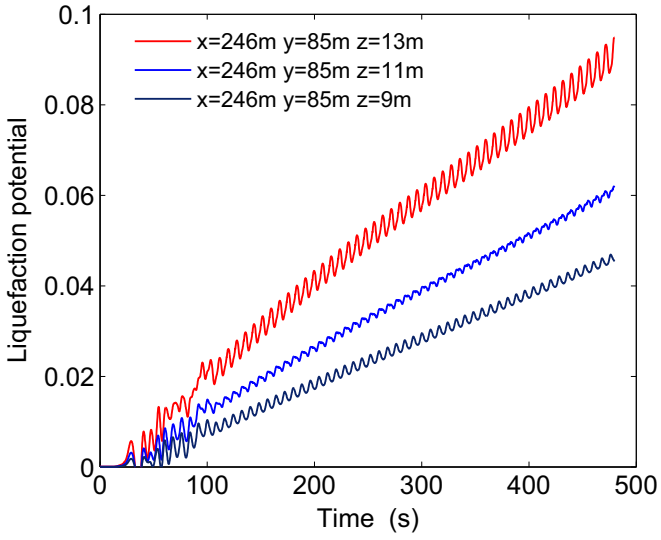

Fig. 14. Liquefaction potential at typical positions on line (x=246 m, y=85 m) behind the breakwater (noted: passing through position D).

between excess residual pore pressure and liquefaction resistance of soil can not reach 1.0. Ishihara [8] suggested that the pore water pressure ratio (p_{excess}/σ_{z0}) in silty sands or sandy silts containing some amount of fines was observed not to develop fully, but instead may stop building up when it has reached a value equal to about 0.9–0.95 of liquefaction resistance. If liquefaction was strictly defined as the occurrence of liquefaction potential being equal to 1.0, then these soils would never 'liquefy' despite of the fact that they may have behaved as a liquefied materials. Some laboratory soil tests [24,9,25] performed at U.C. Berkeley also shown that liquefaction still could occur when the excess residual pore pressure did not reach the initial vertical effective stress. It means that liquefaction is highly possible to occur even if $L_{potential} < 1.0$. Based on this point, we assume that a soil will liquefy if $L_{potential} \geq \alpha_r$. α_r is a coefficient depending on soil characteristics. Its range generally is 0.78–0.99 [24]. Accordingly, liquefaction resistance of a soil can be defined as $L_r = \alpha_r(-\sigma_{z0} + \alpha c)$. In this study, due to the fact that the seabed foundation is assumed as sandy soil, cohesion c is 0.

From the point of view of engineering design, the coefficient α_r also can be deemed as the maximum allowable degree of liquefaction resistance capacity of a soil, for example, α_r could be set as 0.8 in the design of engineering structures. It means that if the degree of liquefaction resistance capacity of seabed foundation is greater than 0.8, coastal engineers involved in design could think the seabed foundation can not support its overlying structures no longer; and overlying offshore structures would lose their instability. In the practice of design engineering, it is highly suggested to set a maximum allowable degree of liquefaction resistance capacity for seabed foundation from case to case according to actual situation.

6.2. Progressive liquefaction prediction

Adopting the definition of liquefaction potential in Eq. (3), the wave-induced residual liquefaction in the seabed foundation around the caisson breakwater is evaluated.

Figs. 12–14 illustrate the time history of wave-induced residual liquefaction potential at some typical positions around the breakwater. In Fig. 12, it can be seen that wave-induced residual liquefaction potential in loose seabed foundation gradually increases until reaching a value near to 1.0. However, residual liquefaction potential at the three typical positions never equals to 1.0. Another phenomenon observed in Fig. 12 is that the time for residual liquefaction potential reaching its highest value along the depth of seabed foundation is

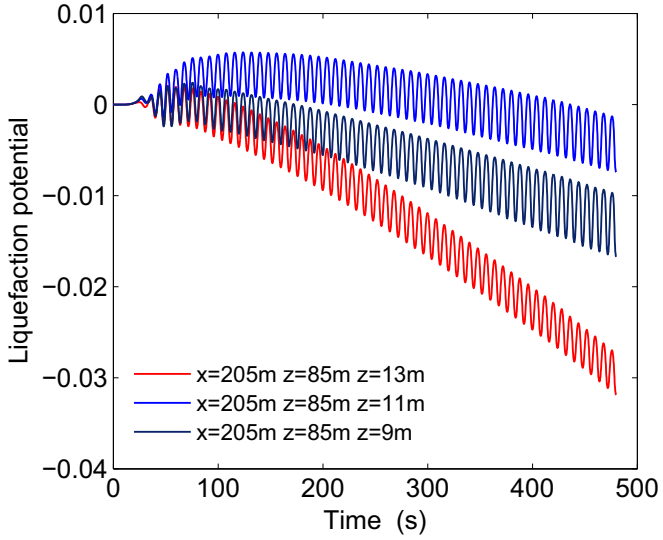

Fig. 15. Liquefaction potential at typical positions on line (x=205 m, y=85 m) under the caisson breakwater (noted: passing through position E).

significantly different. The time needed for residual liquefaction potential to reach its highest value is positively related to buried depth of soil. For example, the time is about 230 s for $L_{potential}$ reaching its highest value when the buried depth is 2 m (z=13 m); while it is about 330 s when the buried depth is 4 m (z=11 m). Until time t=480 s, liquefaction potential does not reach the highest value when the buried depth is 6 m (z=9 m). This characteristics of liquefaction in the seabed foundation in front of the caisson breakwater is the symbol of wave-induced progressive liquefaction.

Figs. 13 and 14 indicate that residual liquefaction potential in the seabed foundation near to the breakwater head, and behind the caisson breakwater is significantly less than that in front of the breakwater at the same time. At time t=480 s, residual liquefaction potential at position C (x=205 m, y=15 m, z=13 m) (near to the head of breakwater) is only about 0.8; and it is only less than 0.1 at position D (x=246 m, y=85 m, z=13 m) (behind the breakwater). Both of them are far away from the liquefaction state. This attributes to the different wave fields around the caisson breakwater.

Fig. 15 demonstrates the time history of wave-induced residual liquefaction potential at three typical positions under the caisson breakwater. It is clearly observed that wave-induced residual liquefaction under the caisson breakwater is negative value. It means that the

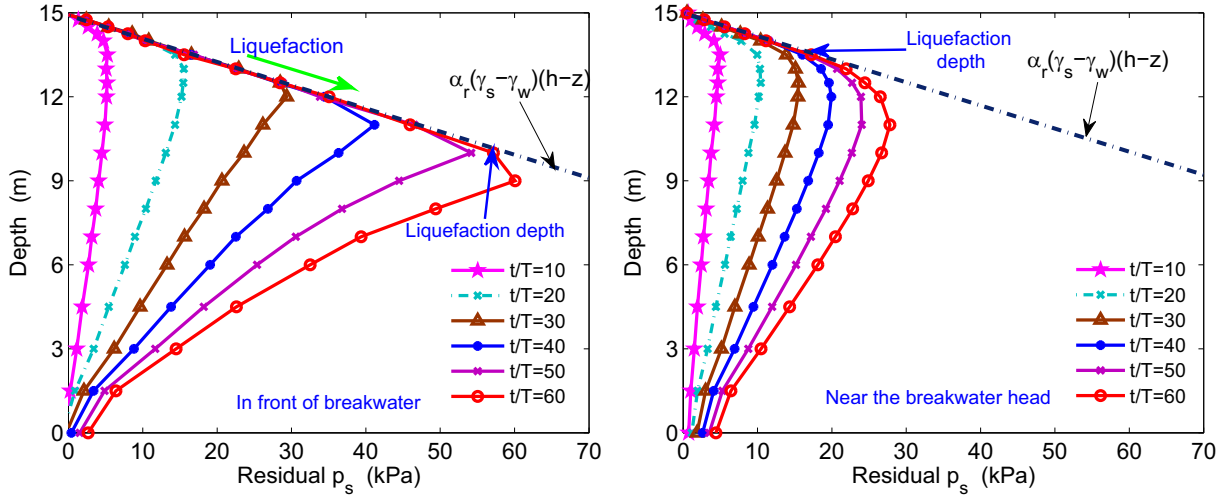

(a) In front of the breakwater (x=164m, y =85m) (b) Near to the breakwater head (x=205m, y=15m)

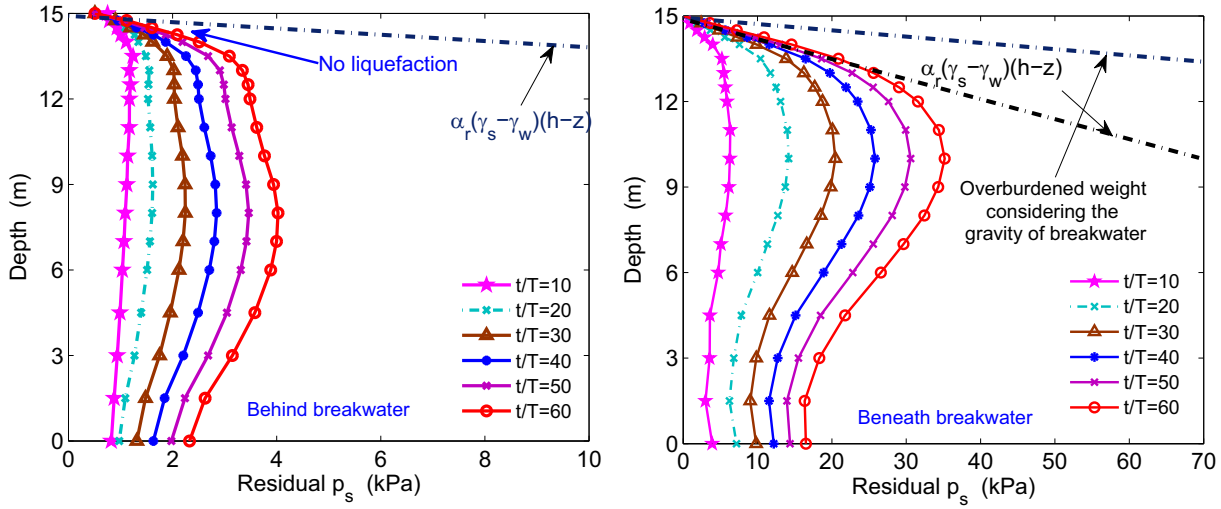

(c) Behind the breakwater (x=246m, y=85m) (d) Under the breakwater (x=205m, y=85m)

Fig. 16. Distribution of the wave-induced residual pore pressure along the depth of the seabed foundation on typical vertical lines around the caisson breakwater at different time. Based on the slope of the liquefaction resistance line in (a) and (b), the coefficient α_r is determined as 0.98 for Nevada dense sand.

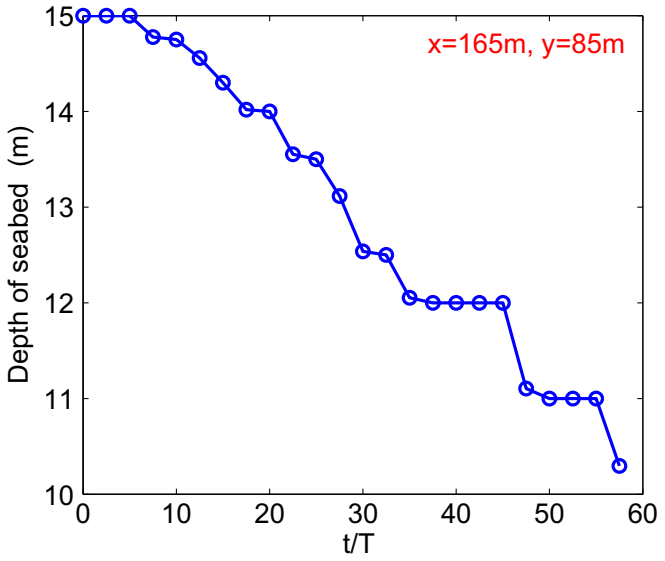

Fig. 17. Wave-induced progressive liquefaction process of seabed foundation at (x=165 m, y=85 m). It is shown that the frontier of liquefaction zone progressively moves downward from the seabed surface.

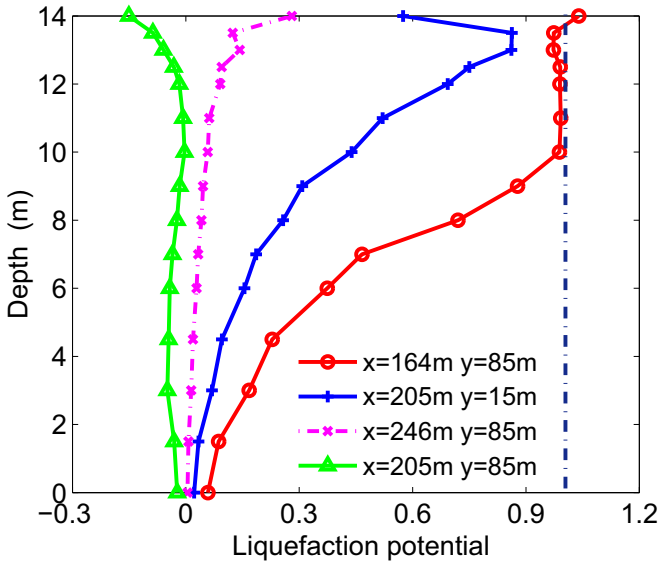

Fig. 18. Distribution of the wave-induced liquefaction potential along the depth of the seabed foundation around the caisson breakwater at time t/T = 60. The coefficient α_r is also determined as 0.98 according to the maximum liquefaction depth in the seabed in front of the caisson breakwater.

wave-induced dynamic effective stresses under the caisson breakwater is compressive (negative value). Actually, the reason for this phenomenon has been analyzed in when analyzing Figs. 11 and 8. In short, seabed foundation under the caisson breakwater is unlikely to liquefy due to the gravity compression of the caisson breakwater.

In the above analysis, it has been recognized that wave-induced residual liquefaction in the seabed foundation is a progressively downward process. Fig. 16 illustrates the progressive liquefaction process on typical vertical lines in the seabed foundation around the caisson breakwater. It is found that wave-induced residual pore pressure builds up with the time of wave loading. However, the build-up of residual pore pressure is subjected to certain constraits. It can not increase indefinitely. There is a line (referred as liquefaction resistance line L_r) in the graphs to show the constrait for the development of residual pore pressure. According to the definition of L_r, this line depends on the initial/current stress state in sand soil.

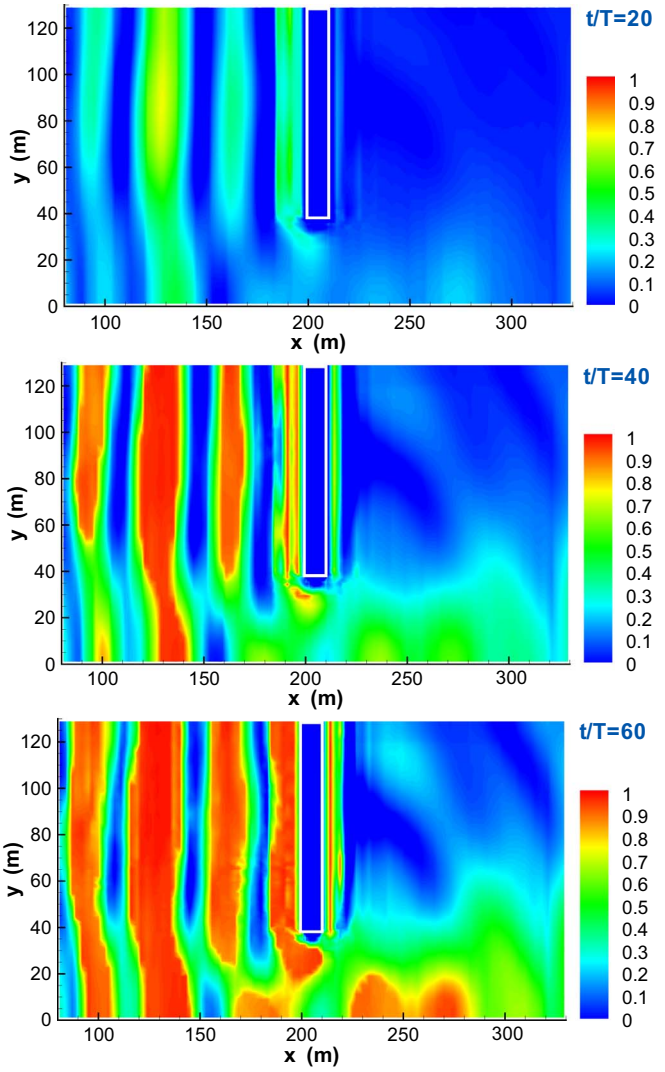

Fig. 19. Distribution of liquefaction potential in the seabed foundation on z=12.5 m

Residual pore pressure can not exceed liquefaction resistance line L_r. When wave-induced residual pore pressure at a position reaches to liquefaction resistance line, it means that the wave-induced excess residual pore pressure overcomes the liquefaction resistance of soil. The soil at this position becomes liquefied at this moment.

In Fig. 16(a), it is clearly observed that wave-induced liquefaction in the seabed foundation in front of the caisson breakwater is a progressive process. The frontier of liquefaction zone in the seabed foundation advances downward gradually, for example, the liquefaction depth is 1.5 m, 3.0 m and 4.0 m, respectively when at time t/T = 20, t/T = 30 and t/T = 50. The progressive liquefaction process on the vertical line (x=165 m, y=85 m) is illustrated in Fig. 17. It is clearly shown that the frontier of liquefaction zone progressively moves downward under long-term wave loading. In Fig. 16(b), it is observed that the maximum liquefaction depth in the seabed near to the breakwater head is only 1.5 m when t/T = 60, which is much less than that in front of the breakwater. Obviously, the reason for this is that standing wave in front of the breakwater is much stronger than the progressive wave. For the seabed foundation behind the breakwater, the diffracted wave-induced residual pore pressure maximumly is only 4 kPa, which is far away from the liquefaction resistance line. The seabed foundation behind the caisson breakwater can not liquefy. Here, the attention is also paid to the seabed foundation beneath the caisson breakwater. In Fig. 16(d), it is observed that residual pore pressure in

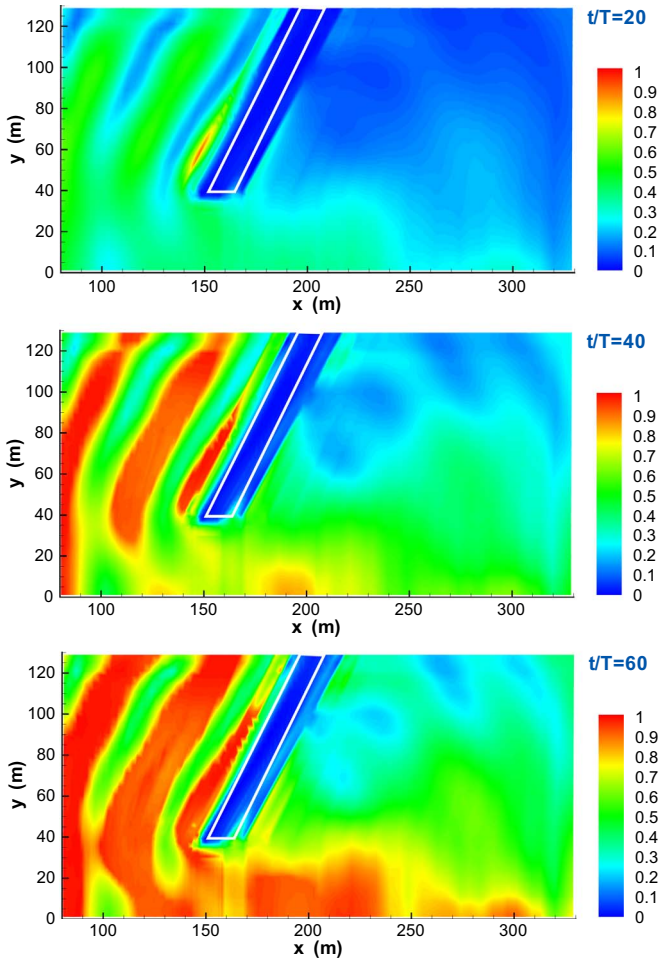

Fig. 20. Distribution of liquefaction potential in the seabed foundation on z=12.5 m when t/T = 20, 40 and 60 for the cases θ = 60°.

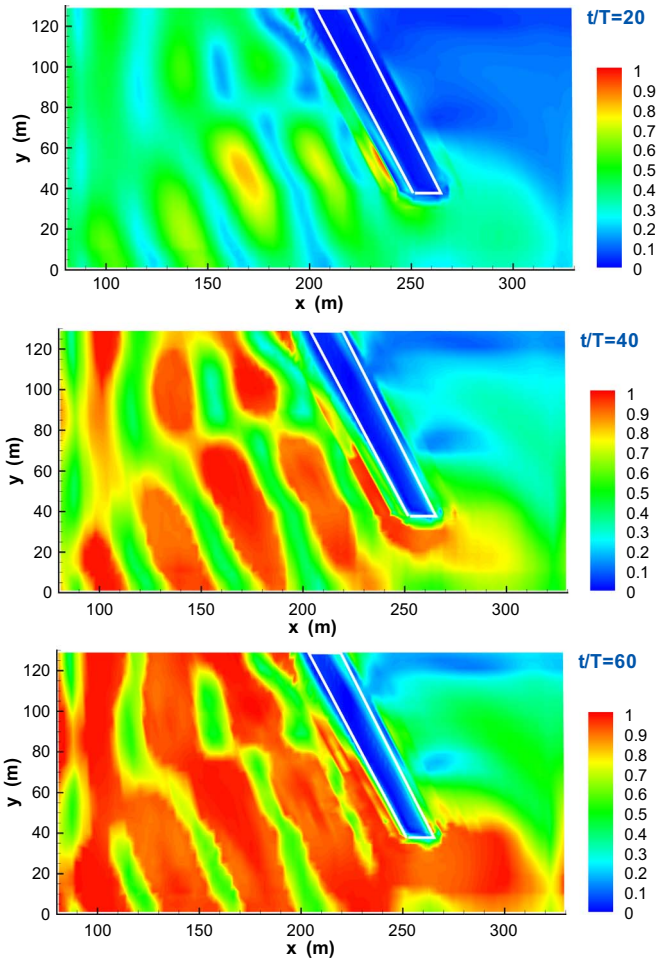

Fig. 21. Distribution of liquefaction potential in the seabed foundation on z=12.5 m when t/T = 20, 40 and 60 for the cases θ = 120°.

the seabed foundation under the breakwater also significantly increase in the process of wave loading. The maximum residual pore pressure can reach up to about 35 kPa in the upper seabed. However, due to the gravity compression of the breakwater, the liquefaction resistance of soil beneath the breakwater significantly increases. The residual pore pressure can not reach the liquefaction resistance line beneath the caisson breakwater. Therefore, it is again shown that seabed soil under the caisson breakwater can not liquefy.

Fig. 18 shows the distribution of wave-induced liquefaction potential along the depth of seabed foundation around the caisson breakwater at time t/T = 60. It is clearly observed that wave-induced liquefaction potential in the upper seabed is greater than that in the lower seabed. In the seabed foundation beneath the caisson breakwater (x=205 m, y=85 m), the liquefaction potential is less than 0.0. It is indicated that the seabed under the caisson breakwater can not liquefy. In the other seabed foundation around the caisson breakwater, the liquefaction potential in front of the breakwater is greatest; and it is smallest behind the breakwater. According to the maximum liquefaction depth in front of the breakwater at time t/T = 60 determined in Fig. 16(a), coefficient α_r is again determined as 0.98. This value of α_r is only valid for Nevada dense sand. For other types of sand bed, α_r should be individually determined.

Fig. 19 shows the distribution of wave-induced residual liquefaction potential in the seabed foundation on the plane z=12.5 m at time t/T = 20, 40 and 60. As illustrated in Fig. 19, residual liquefaction potential in the seabed foundation at time t/T = 60 is significantly greater than that at time t/T=20 and 40. It is indicated that pore pressure in the seabed foundation significantly builds up from time t/T = 20–60. In Fig. 19, it also can be seen that residual liquefaction potential behind the caisson breakwater is much less than that in front of the caisson breakwater at the same time. This phenomenon has also been recognized in the above analysis. The residual liquefaction potential in the seabed foundation under the caisson breakwater is less than zero at time t/T = 20, 40 and 60. This attributes to the fact that the gravity of breakwater compresses the soil beneath it, and makes it is unlikely for the inter-granular effective stresses to reach zero.

Another interesting phenomenon observed in Fig. 19 is that the zones with high and low liquefaction potential appear alternatively in front of the breakwater. This can be attributed to the wave in front of the breakwater is standing wave resulted from the interference between incident wave and reflected wave. Under the nodes of standing wave, the liquefaction potential is high; while it is low under the anti-nodes of standing wave.

7. Effect of the direction of breakwater

The angle between incident wave and the caisson breakwater is set as θ = 60° and θ = 120°, respectively. The 3D waves fields are generated by wave maker adopting the same wave characteristics with the case when θ = 90°: H=1.5 m, d=10 m, and T=8.0 s. The wave field in front of the caisson breakwater is short-crested wave, rather than standing wave if incident waves obliquely propagating to the caisson breakwater. The wave-induced force per meter length acting on the front lateral side of the breakwater is also much smaller than that if the breakwater is perpendicular with incident wave. Different wave fields around the

caisson breakwater directly lead to different distribution of residual liquefaction zone in the seabed foundation around the caisson breakwater.

Figs. 20 and 21 show the 3D distribution of wave-induced residual liquefaction potential on the plane z=12.5 m in the seabed foundation around the caisson breakwater when $\theta = 60°$ and $\theta = 120°$, respectively. Some the same phenomena can be observed when $\theta = 90°$. Residual liquefaction potential in the seabed foundation increases with the time of wave loading. Residual liquefaction potential in the seabed foundation when $t/T = 60$ is significantly greater than that when $t/T = 20$ and 40, and residual liquefaction potential behind the caisson breakwater is much less than that in front of it at the same time. Also due to the compression of the caisson breakwater, residual liquefaction potential beneath the caisson breakwater is apparently small, nearly zero.

Comparing the distributions of residual liquefaction potential shown in Fig. 19 with that shown in Figs. 20 and 21, it is found that the direction of the caisson breakwater indeed has significant effect on the distribution of wave-induced residual liquefaction in the seabed foundation around the caisson breakwater. The zones with high and low residual liquefaction potential distribute alternately in the seabed foundation in front of the caisson breakwater; and they are basically parallel with the direction of the breakwater. In the zones with low residual liquefaction potential, $L_{potential}$ can reach up to 0.5–0.6 when $\theta = 60°$ and $\theta = 120°$. However, $L_{potential}$ in these counterpart zones is nearly zero in the case $\theta = 90°$. Overall, 3D wave-induced residual liquefaction in the seabed foundation in front of the caisson breakwater is most intensive when $\theta = 120°$.

8. Conclusions

The interaction between 3D ocean wave, a caisson breakwater and its loosely deposited seabed foundation is investigated adopting an integrated numerical model FSS-CAS 3D. The interaction mechanism of wave, breakwater and loose seabed foundation is analyzed comprehensively through the presented numerical results. It is indicated that the interaction mechanism of FSSI problme involving loose seabed foundation is much more complicated than that only very dense (elastic) seabed foundation involved. It is also shown that the developed integrated numerical model FSSI-CAS 3D can effectively capture a series of nonlinear characteristics of FSSI problme. It would be a recommendable computational model for FSSI problme involving loose seabed foundation. The followings are some specific summarises from the numerical analysis.

(1) Due to the soil compaction in loose seabed under cyclic wave loading, breakwater built on loose seabed foundation continuously subsides and tilts. The subsidence and tilting of breakwater mainly depend on the magnitude of wave impact, as well as the properties of loose seabed soil.
(2) Under wave loading, pore pressure in loose seabed foundation builds up; and effective stresses between soil particles decrease correspondingly. The rate of pore pressure build up in loose seabed foundation in front of breakwater is much greater than that behind breakwater; and rate of the pore pressure build up in loose seabed foundation is oppositely related to buried depth.
(3) Pore pressure in loose seabed foundation can not build up infinitely. There is a liquefaction resistance line to constrain the development of pore pressure. When wave-induced residual pore pressure at a position reaches liquefaction resistance line, it means that the excess residual pore pressure is sufficient to overcome liquefaction resistance, seabed soil at this position becomes liquefied. The analysis indicates that wave-induced residual liquefaction in front of a breakwater is a progressive process. The liquefaction depth moves downward in loose seabed foundation gradually under wave loading. Seabed foundation beneath breakwater is a unique zone. Pore pressure in this zone also builds up significantly. However, effective stresses between soil particles increase. This phenomenon is completely different from that in other zones around the breakwater. The reason for this phenomenon is that the wave-induced swaying and tilting of breakwater makes the soil particles in the seabed beneath breakwater rearrange themself in a denser way.
(4) Liquefaction analysis indicates that wave-induced residual liquefaction potential is much greater in front of breakwater than that behind breakwater; and their residual liquefaction potential increases with the time of wave loading. The zones with high and low residual liquefaction potential in loose seabed foundation in front of breakwater distribute alternately, and the pattern of the liquefaction zones are parallel with breakwater.
(5) Parametric study indicates that the direction of breakwater has significant effect on the distribution of wave-induced residual liquefaction in loose seabed foundation around breakwater head. This is attributed to that different wave fields are formed around the breakwater head.

Acknowledgements

Dr Ye Jianhong appreciates the financial funding support from National Natural Science Foundation of China under Project no. 41472291. Prof. Wang and Prof. Zhu thank the financial support from Chinese 973 Project: Evolutionary Trends and Sustainable Utilization of Coral Reefs in the South China Sea (2013CB956104). Dr Ye and Prof. Jeng are grateful for the financial support from EPSRC#EP/G006482/1. Dr Ye also appreciates the funding support of Overseas Research Student Award from Scottish Government, UK.

References

[1] Blom FJ. A monolithical fluid-structure interaction algorithm applied to the piston problem. Comput Methods Appl Mech Eng 1998;167(3):369–91.
[2] Cheng L, Sumer BM, Fredsoe J. Solution of pore pressure build up due to progressive waves. Int J Numer Anal Method Geomech 2001;25(9):885–907.
[3] Dunn SL, Vun PL, Chan AHC, Damgaard JS. Numerical modeling of wave-induced liquefaction around pipelines. J Waterw Port Coast Ocean Eng 2006;132(4):276–88.
[4] Farhat C, Lesoinne M. Two efficient staggered algorithms for the serial and parallel solution of three-dimensional nonlinear transient aeroelastic problems. Comput Methods Appl Mech Eng 2000;182(3):499–515.
[5] Groot MBD, Kudella M, Meijers P, Oumeraci H. Liquefaction phenomena underneath marine gravity structures subjected to wave loads. J Waterw Port Coast Ocean Eng ASCE 2006;132(4):325–35.
[6] Hsu JR, Jeng DS. Wave-induced soil response in an unsaturated anisotropic seabed of finite thickness. Int J Numer Anal Methods Geomech 1994;18(11):785–807.
[7] Hur DS, Kim CH, Yoon JS. Numerical study on the interaction among a nonlinear wave, composite breakwater and sandy seabed. Coast Eng 2010;57(10):917–30.
[8] Ishihara K. Liquefaction and flow failure during earthquakes. Géotechnique 1993;43(3):351–451.
[9] Kammerer AM, Pestana JM, Seed RB. Undrained response of monterey 0/30 sand under multidirectional cyclic simple shear loading conditions. Technical report. University of California, Berkeley. Geotechnical Engineering Research Report No. UCB/GT/02-01. 2002.
[10] Kirca VSO, Summer BM, Fredse J. Residual liquefaction of seabed under standing waves. J Waterw Port Coast Ocean Eng 2013;139(6):489–501.
[11] Kudella M, Oumeraci H, Groot MBD, Meijers P. Liquefaction phenomena underneath marine gravity structures subjected to wave loads. J Waterw Port Coast Ocean Eng ASCE 2006;132(4):310–24.
[12] Li J, Jeng DS. Response of a porous seabed around breakwater heads. Ocean Eng 2008;35(8–9):864–86.
[13] Lin ZP, Liu PL-F. Internal wave-maker for navier-stokes equations models. J Waterw Port Coast Ocean Eng 1999;99(4):207–15.
[14] Mizutani N, Mostarfa A, Iwata K. Nonlinear regular wave, submerged breakwater and seabed dynamic interaction. Coast Eng 1998;33:177–202.
[15] Pastor M, Chan AHC, Mira P, Manzanal D, Fernndez MJA, Blanc T. Computational geomechanics: the heritage of olek zienkiewicz. Int J Numer Methods Eng 2011;87(1–5):457–89.
[16] Pastor M, Zienkiewicz OC, Chan AHC. Generalized plasticity and the modelling of soil behaviour. Int J Numer Anal Methods Geomech 1990;14:151–90.
[17] Rahman MS, Jaber WY. Simplified drained analysis for wave-induced liquefaction in ocean floor sands. Soils Found 1986;26(3):57–68.
[18] Sassa S, Sekiguchi H. Wave-induced liquefaction of beds of sand in a centrifuge. Géotechnique 1999;49(5):621–38.
[19] Sassa S, Sekiguchi H. Analysis of wave-induced liquefaction of sand beds.

Géotechnique 2001;51(2):115–26.
[20] Sassa S, Sekiguchi H, Miyamoto J. Analysis of progressive liquefaction as a moving-boundary problem. Géotechnique 2001;51(10):847–57.
[21] Sumer BM, Kirca VSO, Fredsoe J. Experimental validation of a mathematical model for seabed liquefaction in waves. In: Proceedings of the international offshore and polar engineering conference. 2011. p. 1010–8.
[22] Teh TC, Palmer AC, Damgaard JS. Experimental study of marine pipelines on unstable and liquefied seabed. Coast Eng 2003;50(1–2):1–17.
[23] Tsai CP. Wave-induced liquefaction potential in a porous seabed in front of a breakwater. Ocean Eng 1995;22(1):1–18.
[24] Wu J, Kammaerer AM, Riemer MF, Seed RB, Pestana JM. Laboratory study of liquefaction triggering criteria. In: Proceedings of the 13th world conference on earthquake engineering. Vancouver, British Columbia, Canada. 2004. Paper No. 2580.
[25] Wu J, Seed RB, Pestana JM. Liquefaction triggering and post liquefaction deformations of monterey 0/30 sand under uni-directional cyclic simple shear loading. Technical report. University of California, Berkeley. Geotechnical Engineering Research Report No. UCB/GE-2003/01. 2003.
[26] Ye J, Huang D, Wang G. Nonlinear dynamic simulation of offshore breakwater on sloping liquefied seabed. Bull Eng Geol Environ 2016;75(3):1215–25.
[27] Ye J, Jeng D, Wang R, Zhu C. Numerical simulation of the wave-induced dynamic response of poro-elastoplastic seabed foundations and a composite breakwater. Appl Math Model 2015;39:322–47.
[28] Ye J, Jeng DS, Chan AHC, Wang R, Zhu Q. 3D integrated numerical model for fluidcstructures seabed interaction (FSSI): elastic dense seabed foundation. Ocean Eng 2016;115:107–22.
[29] Ye J, Wang G. Numerical simulation of the seismic liquefaction mechanism in an offshore loosely deposited seabed. Bull Eng Geol Environ 2016;75(3):1183–97.
[30] Ye JH. 3D liquefaction criteria for seabed considering the cohesion and friction of soil. Appl Ocean Res 2012;37:111–9.
[31] Ye JH, Jeng D-S, Chan AHC. Consolidation and dynamics of 3D unsaturated porous seabed under rigid caisson breakwater loaded by hydrostatic pressure and wave. Sci China Technol Sci 2012;55(8):2362–76.
[32] Ye JH, Jeng D-S, Wang R, Zhu CQ. A 3-D semi-coupled numerical model for fluidstructures seabed-interaction (FSSI-CAS 3D): model and verification. J Fluids Struct 2013;40:148–62.
[33] Ye JH, Jeng D-S, Wang R, Zhu CQ. Validation of a 2D semi-coupled numerical model for fluid-structures-seabed interaction. J Fluids Struct 2013;42:333–57.
[34] Ye JH, Wang G. Seismic dynamics of offshore breakwater on liquefiable seabed foundation. Soil Dyn Earthq Eng 2015;76:86–99.
[35] Zhang XY, Lee FH, Leung CF. Response of caisson breakwater subjected to repeated impulsive loading. Géotechnique 2009;59(1):3–16.
[36] Zienkiewicz OC, Chan AHC, Pastor M, Schrefler BA, Shiomi T. Computational geomechanics with special reference to earthquake engineering. England: John Wiley and Sons; 1999.